Thin-Film light-trapping enhanced Quantum Dot photovoltaic cells (TFQD): an enabling technology for high power-to-weight ratio space solar arrays
Grant agreement No. 687253
Start date: January 1st, 2016 – Duration: 24 months

Deliverable D3.1 – WP3
Wafer-based QD solar cell with 100 QD layers with density of ~10^{11} cm^{-2}

Lead Partner: UCL

Contributing Partners: RBU

Version: 1.1
Revision Date: 21st October 2016
Deliverable Type: RTD
Delivery date: 31st October 2016
Nature of the Deliverable: (R)eport
Dissemination Level: PUBLIC

Abstract

The present document provides a report on the deliverable D3.1, the wafer-based quantum dot solar cell with 100 quantum dot layers with in-plane quantum dot density of $\sim 10^{11}$ cm^{-2}. This document provides a detailed description of the material optimisation for quantum dot solar cells with high short-circuit current by incorporating high-density quantum dots.

Disclaimer

The information, documentation and figures available in this deliverable are written by the TFQD Consortium partners under EC co-financing and does not necessarily reflect the view of the European Commission.
The information in this document is provided "as is", and no guarantee or warranty is given that the information is fitting any particular purpose.
The user uses the information at its sole risk and liability.

Change Records

Table 1–1 Change records of current document

Issue	Date	Change Record	Author(s)
1.0 (Draft)	27/09/2016	Draft	D. Kim J. Wu H. Liu
1.1	21/10/2016	First Release	D. Kim J. Wu H. Liu

Table of Contents

List of Figures

List of Tables

List of Acronyms

AFM*: Atomic force microscopy*
DJ*: Deep-junction*
EQE*: External quantum efficiency*
FF*: Fill factor*
IB*: Intermediate band*
IBSC*: Intermediate band solar cell*
Jsc: Short-circuit current
J-V*: Current density-voltage*
MBE*: Molecular beam epitaxy*
QD*: Quantum dot*
QDSC*: Quantum dot solar cell*
SC*: Solar cell*
SJ*: Shallow-junction*
TEM*: Transmission electron microscopy*
TFQD*: Thin-film quantum dot*
Voc*: Open-circuit voltage*
XRD*: X-ray diffraction*

1. INTRODUCTION

Since the first proposal of the intermediate band solar cells (IBSCs) by Luque and Martí [1], [2] in 1997, QDs have been drawing much attention as intermediate band (IB) materials. The zero density of states and three-dimensional quantum confinement nature make QDs ideal candidates for the IB materials for high efficiency IBSCs. In particular for space applications, where end-of-life performance is critical, QDSCs have an additional advantage of having an enhanced radiation tolerance when compared with bulk SCs. Studies have demonstrated two-photon transitions via IB by incorporating InAs QDs in the intrinsic region of a GaAs p-i-n single junction structure, where the IB is formed by QDs [3]–[5]. However, despite the great potential held by QDs, the promise of high efficiency QD-IBSCs has not yet been realised.

One of the objectives of TFQD is to develop thin-film light-trapping enhanced QDSCs with a high power conversion efficiency of over 30 %. For a QDSC to have such high-efficiency, it is essential to increase the photon absorption in QD arrays. To this end, the plasmonic materials have been investigated [6]–[8]. Another alternative for increasing QD photon absorption is to increase the number of QDs by growing high-stack QD layers [9], or high in-plane density QD layers using Sb-mediated QD growth technique, as previously reported by UCL [10]. However, to date, QDSCs with both high number of QD layers, and high in-plane QD density ($\sim 10^{11}$ cm^{-2}) have not been demonstrated.

In this deliverable (D3.1), the material optimisation for the high-stack InAs/GaAs QDSCs with high in-plane QD density is reported. Section 2 describes the optimisation steps involved during and prior to the growth of the QDSC structure using molecular beam epitaxy (MBE), and Section 3 discusses the results from the solar cell performance measurements, including current density-voltage (*J-V*) characteristics and external quantum efficiency (*EQE*).

2. GROWTH OF HIGH-DENSITY QUANTUM DOT SOLAR CELLS USING MOLECULAR BEAM EPITAXY

As specified in WP3 D3.1, the growth of high-stack QDSC structure with 100 QD layers and high-in plane QD density has been achieved. All samples were grown using a solid-source MBE on n+ GaAs (1 0 0) substrates. The growth details, including the calibration steps involved prior to the QDSC samples, are described in this section.

2.1. Growth calibrations for quantum dot solar cell structure with high in-plane quantum dot density

InAs QD growth of high in-plane density by using the Sb-mediated growth technique. Sb deposited below the QD layers has been found to work as an active surfactant and form small islands on GaAs layers, which lead to the formation of nucleation sides for InAs QD growth, and hence high QD density. To obtain high density QDs, a series of samples that consist of buried QD layers sandwiched by GaAs spacer layers, and an uncapped surface QD layer were grown with different amounts of Sb irradiation, InAs coverage, and QD growth temperatures. For all samples, high-growth-temperature GaAs spacer layers were used in order to suppress the formation of threading dislocations.
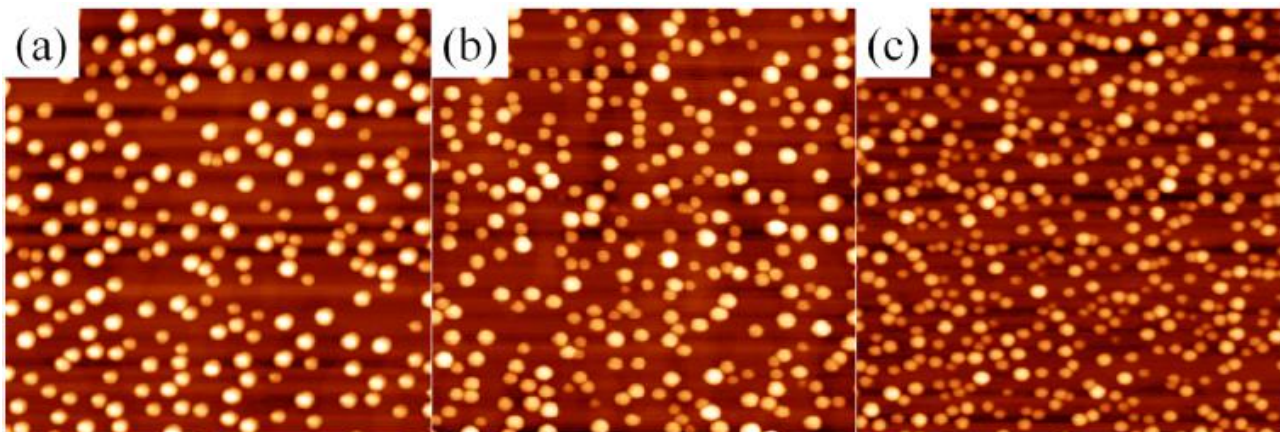
Figure 1 AFM images (1 x 1 μm^2) of 2.1 ML InAs QDs grown at 500 ℃ on GaAs with (a) no Sb, (b) 3 ML Sb, and (c) 6 ML Sb [10].

Figure 1 shows the atomic force microscopy (AFM) images of the QD samples grown with different Sb coverages, from the previous study performed at UCL [10]. Without any supply of Sb, the QD density is estimated to be ~2.30×10^{10} cm^2. A significant improvement in the QD density is observed after Sb deposition, with increased QD density of ~2.90×10^{10} cm^2 for 3 ML Sb sample, and ~4.40×10^{10} cm^2 for 6 ML Sb sample. The increase of QD density can be attributed to the Sb atoms segregated at the growth front [11]. In other words, the Sb atoms work as an active surfactant that bonds to the GaAs layer and forms small islands. Moreover, the supply of Sb leads to an increase in the step densities on the GaAs surfaces. The islands and surface steps formed by supplying Sb on GaAs surface reduce the In adatom diffusion length and create nucleation sites for InAs QD growth. Consequently, Sb-mediated QD growth has resulted in an increase in the QD density.

2.1.1. InAs coverage

In order to determine the optimal InAs coverage for high QD density, QD structures with InAs coverages ranging from 2.05 to 2.35 ML were grown at a fixed growth temperature of 530 ºC. Sb coverage remained at 6 ML for all samples. Figure 2 (a) and (b) are the AFM images of QDs grown using InAs coverages of 2.05 ML and 2.35 ML, respectively. With low InAs coverages of 2.05 ML, the sample has an almost defect-free surface and QD density of ~3.34×10^{10} cm^2. An increase in InAs coverage leads to higher QD density of ~4.91×10^{10} cm^2. Despite the slight increase in the number of defective clusters, the cluster density for all samples still remained relatively low (~1.0×10^8 cm^2).

(a)　　　　　　　　(b)

2.05 ML InAs　　　2.35 ML InAs
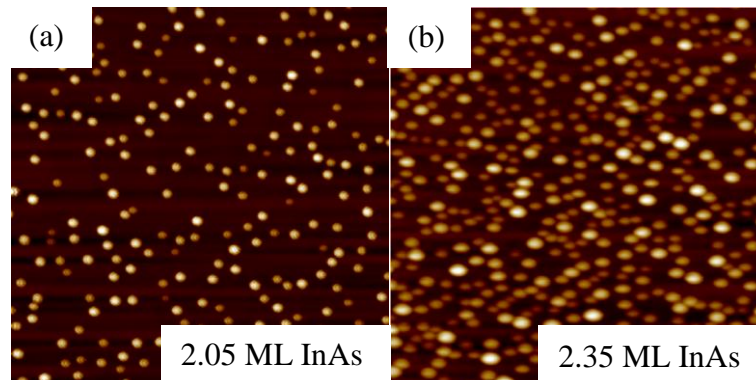
Figure 2 AFM images (1 x 1 μm^2) of (a) 2.05 ML and (b) 2.35 ML InAs QDs grown at 530 ºC on GaAs with 6 ML Sb.

← Low InAs coverage	InAs coverage: 2.35 ML	High InAs coverage →
Lower QD density	High QD density	Higher QD density
Defect free	Low defect density	Higher defect density

Figure 3 Initial InAs coverage optimisation: the influence of InAs coverage on the QD density and defect density.

2.1.2. QD growth temperature

The influence of the QD growth temperature on the QD morphology have also been studied. Samples were grown at different temperatures ranging from 490 to 510 ℃, whilst keeping the same Sb coverage (6 ML), and the high InAs coverage (2.35 ML) that led to an improvement in the QD density. Figure 4 (a), (b), and (c) are the AFM images of InAs QDs deposited at 490, 500, and 510 ℃, respectively The decrease in growth temperature leads to formation of smaller and denser QDs. The in-plane QD density increased to $\sim 6.35 \times 10^{10}$ cm^2 at the growth temperature of 500 ℃, and $\sim 9.08 \times 10^{10}$ cm^2 at the growth temperature of 490 ℃. The reduction in In adatom diffusion length at lower growth temperatures is believed to contribute to this increase in QD density. However, this also led to a significant increase in the number of defective large clusters, as shown in Figure 4 (a). The appearance of large clusters is due to the coalescence of small dots [12], which results in large clusters and then misfit dislocations.
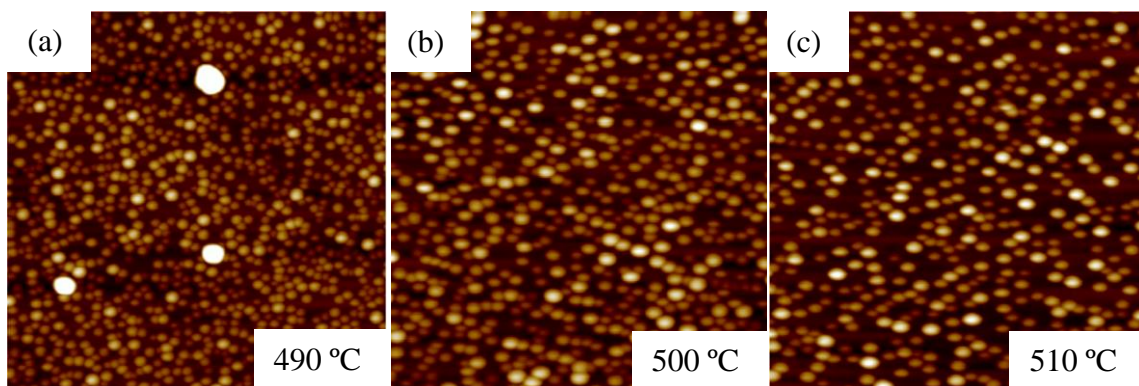
Figure 4 AFM images (1 x 1 µm^2) of 2.35 ML InAs QDs grown at (a) 490 ℃, (b) 500 ℃, and (c)510 ℃ on GaAs with 6 ML Sb.

← Low temperature	Growth temperature: 490 ºC	High temperature →
High defect density	Low defect density	Lower defect density
Higher QD density	High QD density	Low QD density
Smaller QDs	QD height: ~ 5nm QD diameter: 25-35 nm	Larger QDs

Figure 5 QD growth temperature optimisation: the influence of QD growth temperature on the QD density, defect density, and QD dimensions.

2.1.3. Sb coverage

The defective clusters are non-radiative recombination centres that decrease the carrier lifetime. Studies have shown that GaAsSb acts as a strain-reducing layer on InAs QDs, which improves the crystal quality and dot density, and reduces the formation of coalescent dots [13]–[15]. This leads to enhanced optical properties of the QD region and reduced non-radiative recombination. Therefore, in order to suppress the coalescence whilst keeping the high QD density, Sb coverages ranging from 6 to 9 ML were used at the growth temperature of 490 ºC, at which high QD density was achieved. Figure 6 (a) and (b) are the AFM images of InAs QDs deposited on 6 and 9 ML, respectively. The QD densities are estimated to be ~9.08×10^{10} cm^2 with Sb coverage of 6 ML, and ~9.39×10^{10} cm^2 with Sb coverage of 6 ML. Fewer defective clusters are observed for the sample with 9 ML Sb. The inference that can be drawn from this is that having higher Sb coverage is favourable in terms of the QD morphology and density. However, this comes with the cost of decreasing the QD size.
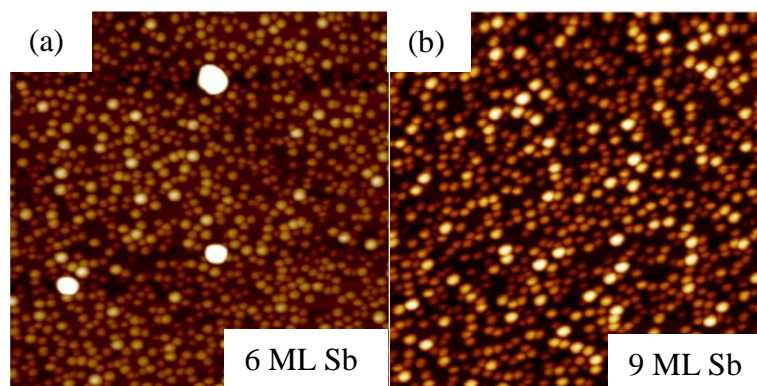
Figure 6 AFM images (1 x 1 µm^2) of 2.35 ML InAs QDs grown at 490 ºC on GaAs with (a) 6 ML Sb and (b) 9 ML Sb

← Low Sb coverage	Sb coverage: 9 ML	High Sb coverage →
High defect density	Low defect density	Lower defect density
Low QD density	Low defect density	Higher QD density
Larger QDs	QD height: ~ 5nm QD diameter: 25-35 nm	Smaller QDs

Figure 7 Sb coverage optimisation: the influence of Sb coverage on the QD density, defect density, and QD dimensions.

2.1.4. InAs coverage (further optimisation)

In order to further improve the QD morphology, InAs coverage has been further optimised. For this, three Sb-mediated InAs/GaAs QD structures were grown with InAs coverages of 2.2, 2.275, and 2.35 ML, as shown in Figure 8. The growth temperature and the Sb coverage for all samples remained the same at 490 ºC and 9 ML Sb, respectively. Although the QD density clearly increases with increasing InAs coverage (~6.31×10^{10} cm^2 for 2.2 ML InAs, ~8.14×10^{10} cm^2 for 2.275 ML InAs, and ~9.39×10^{10} cm^2 for 2.35 ML InAs), this comes with the cost of higher defect density. Therefore, the growth conditions were determined in a way to maximise the density and the size of the QDs without significantly deteriorating the QD morphology. Below are the optimised conditions for the Sb-mediated InAs QD growth with high in-plane QDs density (~8.14×10^{10} cm^2):

- InAs coverage: 2.35 ML
- Growth Temperature: 490 °C
- Sb coverage: 6 ML.
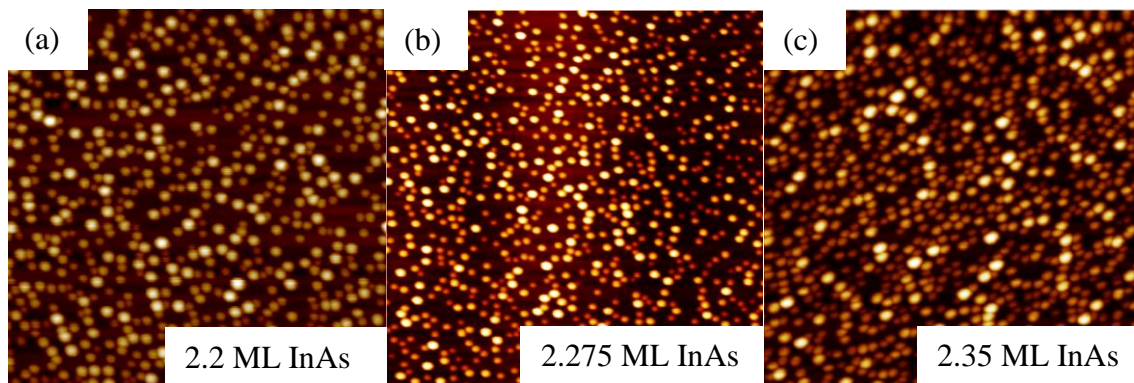
Figure 8 AFM images (1 x 1 μm^2) of (a) 2.2 ML, (b) 2.275 ML, and (c) 2.35 ML InAs QDs grown at 490 ºC on GaAs with 9 ML Sb.

← Low InAs coverage	InAs coverage: 2.275 ML	High InAs coverage →
Lower QD density	High QD density	Higher QD density
Defect free	Low defect density	Higher defect density

Figure 9 Further InAs coverage optimisation: the influence of InAs coverage on the QD density and defect density.

2.2. Growth calibrations for quantum dot solar cells with high-stack quantum dot layers

Using the optimised growth conditions for high in-plane QD density, a high-stack (× 100 layers) InAs/GaAs QD structure was grown, as shown in Figure 10. No strain-balancing technique was employed, and an additional layer of QDs were also grown on the top surface for AFM measurements.

Figure 11 (a) and (b) show the surface morphology of InAs QDs grown on 1 layer and 100 layers of InAs/GaAs QD structures, respectively. The AFM results show high in-plane QD density of over 8 × 10^{10} cm^2 even after the growth of 100 stacks of QD layers.
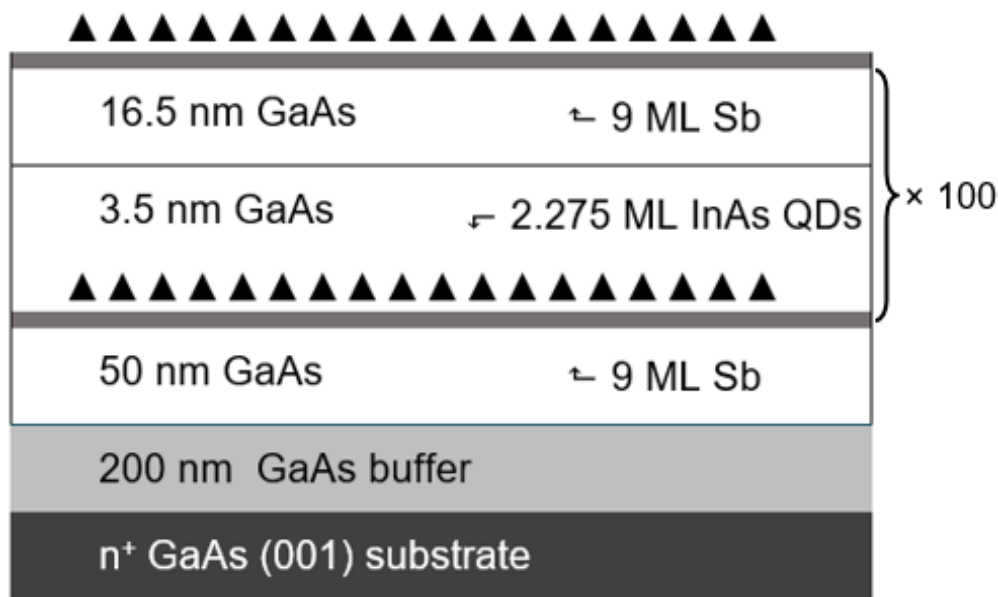
Figure 10 Structure of the high-stack (100-stack) InAs/GaAs QD structure with high in-plane QD density using Sb-mediated growth technique.
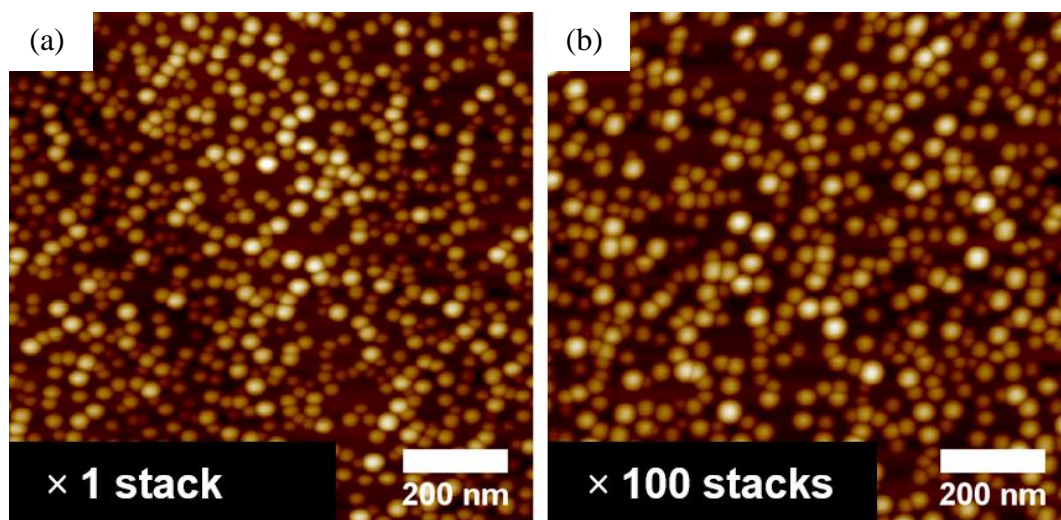
Figure 11 AFM images of InAs QDs (Sb-mediated growth) for (a) 1-stack and (b) 100-stack InAs/GaAs QD structures.

Although the direct measurements of QD heights was difficult due to the high QD density, the estimated QD height distribution could be obtained by performing AFM surface roughness analysis, as shown in Figure 12. For both 1 QD and 100 QD samples, QD sizes show bimodal distributions, with average smaller and larger QD sizes of ~ 2 nm and ~5 nm, respectively. The average QD height for 1 QD sample (4.43 nm) is estimated to be slightly higher than that of 100 QD sample (4.17 nm), however, this is not a sole representation of the change in the QD density as the QD heights show bimodal distribution. The bimodal distribution of QD heights becomes more evident with the high-stack InAs/GaAs QD structure. This agrees well with the PL spectra shown in Figure 13, where the emission peaks of the larger QDs (~ 1000 nm) and the smaller QDs (~ 970 nm) are more comparable for 100 QD sample than 1 QD sample.
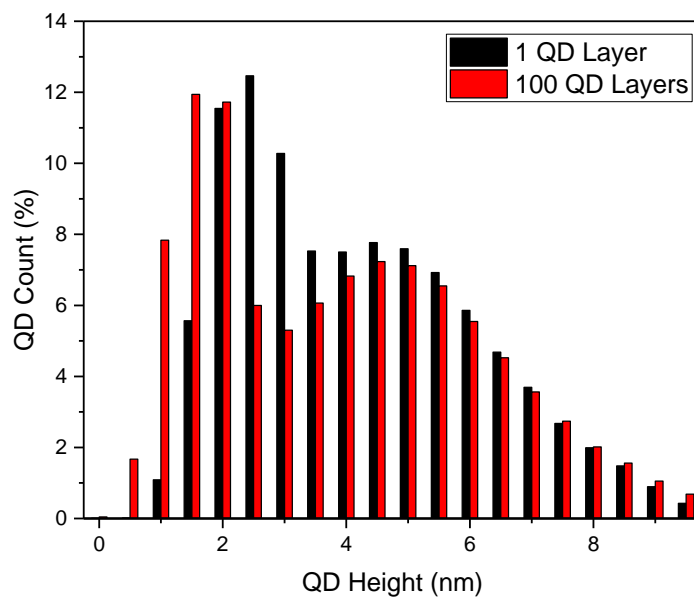
Figure 12 Height histograms of InAs QDs (Sb-mediated growth) in 1-stack and 100-stack InAs/GaAs QD structures.
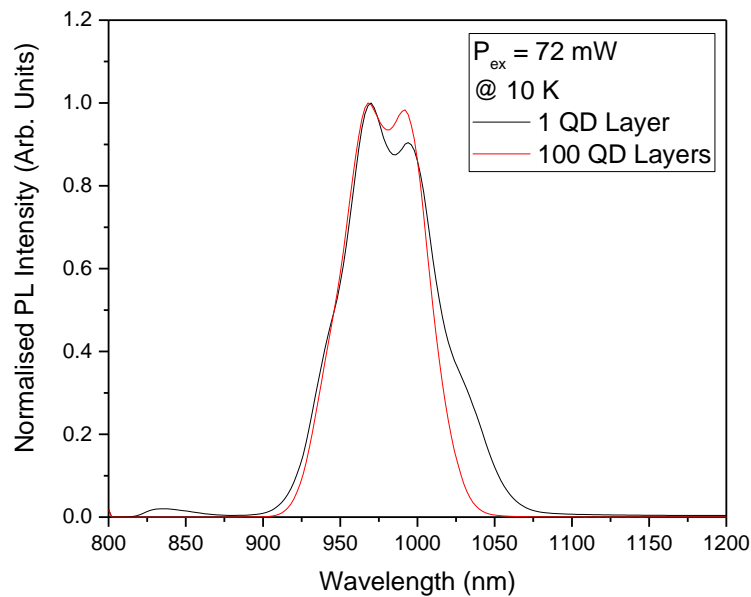
Figure 13 Normalised PL spectra of the 1-stack and 100-stack InAs/GaAs QD structures measured at 10 K.

Transmission electron microscopy (TEM) measurements have also been performed to examine the change in the material quality along the growth direction. Figure 14 (a), (b), and (c) show the whole structure, top 20 layers, and middle 20 layers of the 100-stack InAs/GaAs QD structure, respectively. Although the TEM images show a good material quality in the lower half of the structure, the upper half suffers from gradual decrease in the material quality as the number of QD layers increases. The top 20 layers, in particular, show a significant deterioration of crystal quality, which indicates a large number of non-radiative recombination centre in presence. This is mainly attributed to the accumulation of the strain from the QDs, however, the possibility of the growth conditions being not fully optimised due to characterisation tools not being available (e.g. X-ray diffraction (XRD) at the time of the material growth cannot be ruled out.
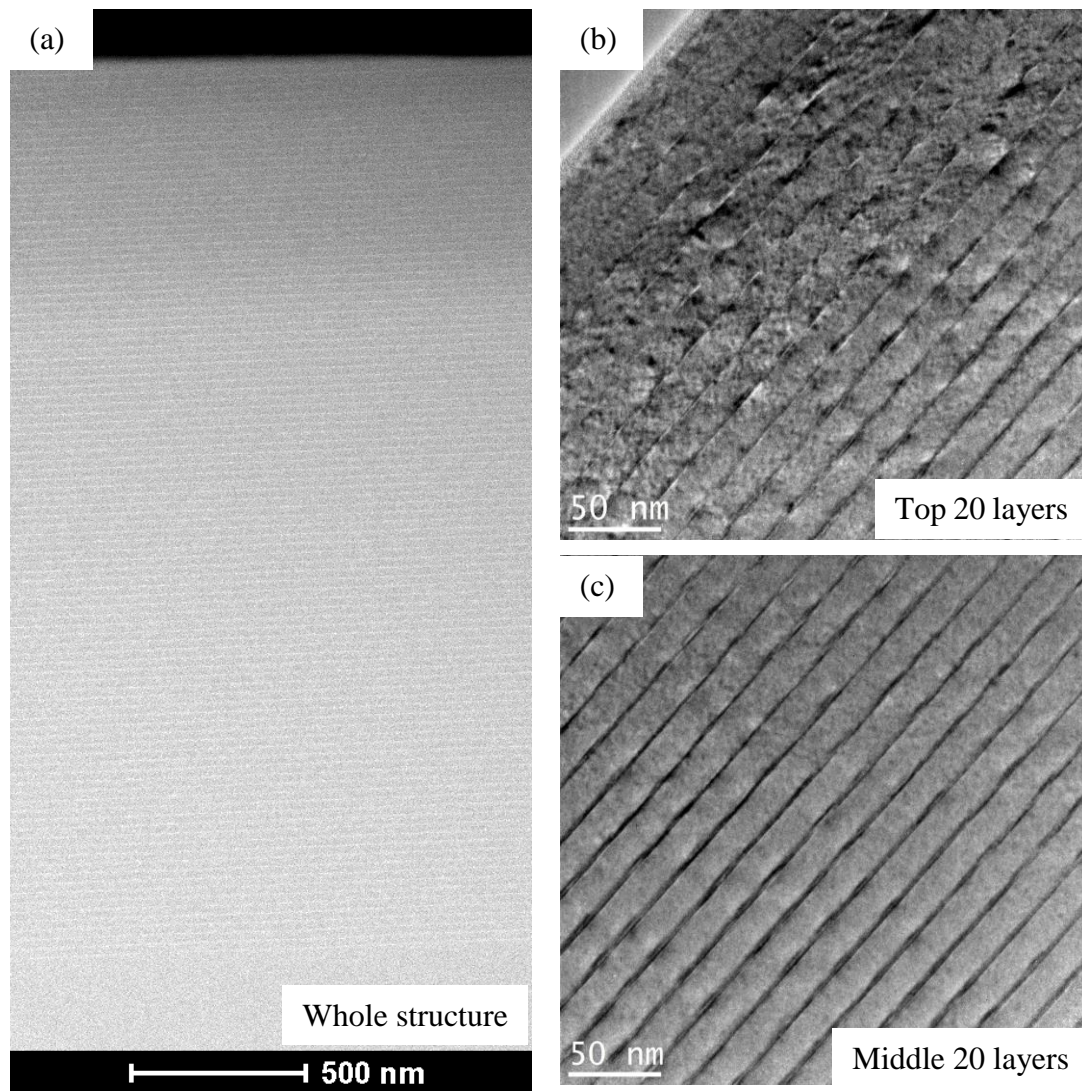
Figure 14 TEM images of 100-stack InAs/GaAs QD structure, showing (a) the whole structure, (b) top 20 layers, and (c) middle 20 layers.

2.3. Solar cell structures

Based on the growth calibrations described above, the epilayer structures for wafer-based regular SCs and QDSCs were grown at UCL (see WP3), and delivered to RBU. The schematics of the epi-structures are shown in Figure 15 to Figure 19.

300 nm n$^+$ GaAs contact	[Si: 1 × 10^{19} cm^{-3}]
20 nm n AlInP window	[Si: 3.4 × 10^{17} cm^{-3}]
2000 nm n$^-$ GaAs emitter	[Si: 1 × 10^{17} cm^{-3}]
100 nm p GaAs base	[Be: 5 × 10^{17} cm^{-3}]
75 nm p Al$_{0.2}$Ga$_{0.8}$As BSF	[Be: 5 × 10^{17} cm^{-3}]
200 nm p+ GaAs contact	[Be: 6 × 10^{18} cm^{-3}]
p$^+$ GaAs (001) substrate	

Figure 15 Schematic of n-on-p DJ SC

300 nm n$^+$ GaAs contact	[Si: 1 × 10^{19} cm^{-3}]
20 nm n AlInP window	[Si: 3.4 × 10^{17} cm^{-3}]
100 nm n$^-$ GaAs emitter	[Si: 1 × 10^{17} cm^{-3}]
2000 nm p GaAs base	[Be: 5 × 10^{17} cm^{-3}]
75 nm p Al$_{0.2}$Ga$_{0.8}$As BSF	[Be: 5 × 10^{17} cm^{-3}]
200 nm p+ GaAs contact	[Be: 6 × 10^{18} cm^{-3}]
p$^+$ GaAs (001) substrate	

Figure 16 Schematic of n-on-p SJ SC

300 nm n⁺ GaAs contact	[Si: 1 × 10^{19} cm^{-3}]
20 nm n AlInP window	[Si: 3.4 × 10^{17} cm^{-3}]
1530 nm n⁻ GaAs emitter	[Si: 1 × 10^{17} cm^{-3}]
16.5 nm i GaAs	[Undoped]
3.5 nm i GaAs	[Undoped]
20 nm i GaAs	[Undoped]
50 nm n⁻ GaAs emitter	[Si: 1 × 10^{17} cm^{-3}]
100 nm p GaAs base	[Be: 5 × 10^{17} cm^{-3}]
75 nm p Al$_{0.2}$Ga$_{0.8}$As BSF	[Be: 5 × 10^{17} cm^{-3}]
200 nm p+ GaAs contact	[Be: 6 × 10^{18} cm^{-3}]
p⁺ GaAs (001) substrate	

× 20

2.275 ML InAs QDs on 9 ML Sb

Figure 17 Schematic of n-on-p DJ QDSC (× 20 QD layers)

300 nm n⁺ GaAs contact	[Si: 1 × 10^{19} cm^{-3}]
20 nm n AlInP window	[Si: 3.4 × 10^{17} cm^{-3}]
930 nm n⁻ GaAs emitter	[Si: 1 × 10^{17} cm^{-3}]
16.5 nm i GaAs	[Undoped]
3.5 nm i GaAs	[Undoped]
20 nm i GaAs	[Undoped]
50 nm n⁻ GaAs emitter	[Si: 1 × 10^{17} cm^{-3}]
100 nm p GaAs base	[Be: 5 × 10^{17} cm^{-3}]
75 nm p Al$_{0.2}$Ga$_{0.8}$As BSF	[Be: 5 × 10^{17} cm^{-3}]
200 nm p+ GaAs contact	[Be: 6 × 10^{18} cm^{-3}]
p⁺ GaAs (001) substrate	

× 50

2.275 ML InAs QDs on 9 ML Sb

Figure 18 Schematic of n-on-p DJ QDSC (× 50 QD layers)

300 nm n⁺ GaAs contact	[Si: 1 × 10^{19} cm^{-3}]
20 nm n AlInP window	[Si: 3.4 × 10^{17} cm^{-3}]
16.5 nm i GaAs	[Undoped]
3.5 nm i GaAs	[Undoped]
20 nm i GaAs	[Undoped]
50 nm n⁻ GaAs emitter	[Si: 1 × 10^{17} cm^{-3}]
100 nm p GaAs base	[Be: 5 × 10^{17} cm^{-3}]
75 nm p Al$_{0.2}$Ga$_{0.8}$As BSF	[Be: 5 × 10^{17} cm^{-3}]
200 nm p+ GaAs contact	[Be: 6 × 10^{18} cm^{-3}]
p⁺ GaAs (001) substrate	

× 100

2.275 ML InAs QDs on 9 ML Sb

Figure 19 Schematic of n-on-p DJ QDSC (× 100 QD layers)

D3.1 – PUBLIC
Version 1.1 of 21st October, 2016
Page n. 18 of 20

3. SOLAR CELL PERFORMANCES

The wafer-based regular and QD cell devices were produced by RBU from a first set of epi-structures delivered by UCL, shown in Figure 15 to Figure 19. At least five 0.25 cm^2 cells (grid coverage 15.9%) and two 1 cm^2 cells (grid coverage 9.5%) were produced from each wafer. No anti-reflection coating was applied during the device fabrication. The solar cell devices were characterised by performing 1-sun (AM1.5) *J-V* and EQE measurements at RBU. The results of the best device from each sample are presented in Figure 20.
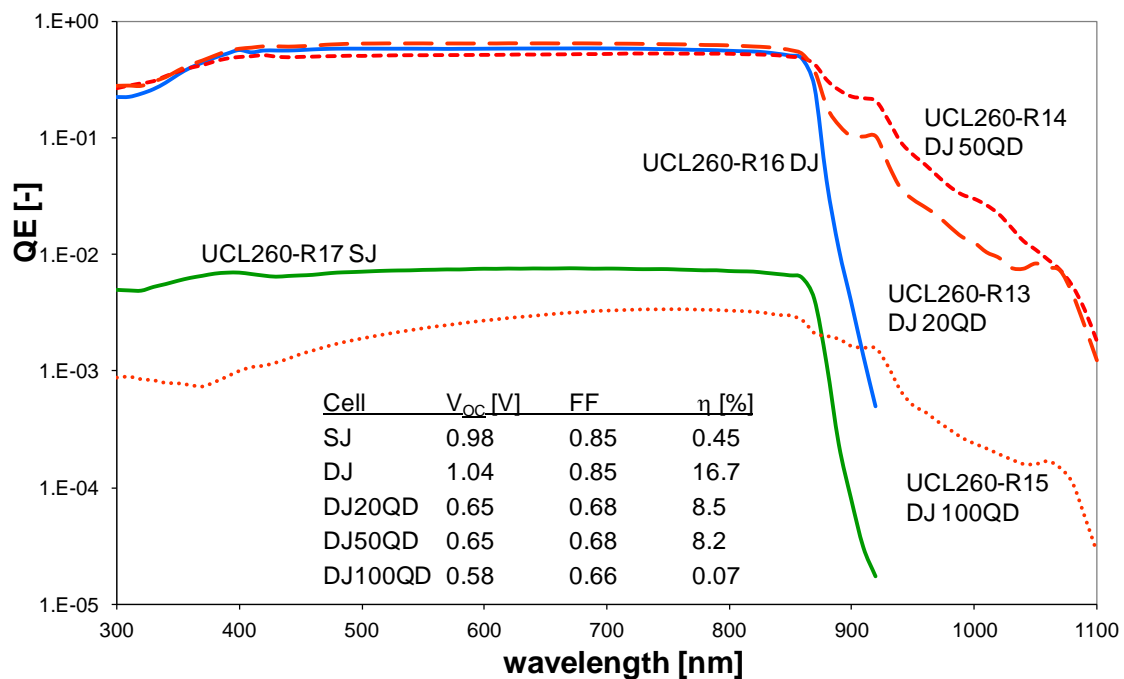

Cell	V_{OC} [V]	FF	η [%]
SJ	0.98	0.85	0.45
DJ	1.04	0.85	16.7
DJ20QD	0.65	0.68	8.5
DJ50QD	0.65	0.68	8.2
DJ100QD	0.58	0.66	0.07

Figure 20 EQE analysis and results from 1 sun AM1.5 J-V measurements of the best cells produced form each epi-layer structure investigated.

Whilst the best device from the shallow-junction (SJ) structure has a good open-circuit voltage (V_{oc}) and fill factor (FF), all cells suffer from extremely low short-circuit current (J_{sc}). This indicates that the proposed design, with low doping level of the emitter with respect to the base, has a very low collection efficiency under a short-circuit condition. On the other hand, deep-junction (DJ) solar cell devices exhibit good J_{sc} (18-19 mA/cm^2), although most of them, 1 cm^2 cells in particular, display low FF and/or low V_{oc}. However, two 0.25 cm^2 cells have relatively high power conversion efficiencies exceeding 16.5%, which suggests that achieving efficiency larger than 22% efficiency is highly probable with ARC and optimised grid coverage. In view of the good device performance achieved with the DJ SC, SJ SC structure will not be considered further.

The DJ QDSCs with 20 and 50 layers of QDs show reduced FF (0.68) and V_{oc} (0.65 V) when compared with the regular SCs. As expected, 50-layer QDSC display higher sub-bandgap EQE due to increased QD absorption. However, the gain in the sub-bandgap absorption is undermined by the loss in the supra-bandgap absorption caused by strain-induced defects, which leads to a slight reduction in the J_{sc}, and hence, cell efficiency.

Increasing the number of QD layers to 100 led to a further reduction in the FF (0.66) and V_{oc} (0.58 V). In addition, the EQE showed totally deteriorated absorption in both the sub-bandgap and supra-bandgap regions. This is attributed to a very high strain-induced defect density in the epilayers, which suggests the need for strain-balancing for high-stack QDSCs.

4. CONCLUSIONS AND NEXT STEPS

In conclusion, the MBE growths for the high-stack InAs/GaAs QDSC structures with high-in plane QD density specified in WP3 have been achieved. High in-plane density InAs QDs could be grown by using the Sb-mediated QD growth technique, where Sb deposited below the QD layers works as an active surfactant and form small islands on GaAs layers. This in turn creates nucleation sites for InAs QD growth, and hence high QD density can be achieved.

The growth conditions for high-density InAs QDs have been calibrated varying the InAs coverage, QD growth temperature, and Sb coverage. Firstly, samples with different InAs coverages have been grown to determine the optimal level. AFM results showed higher QD density for the sample with higher InAs coverage. However, the increase in the QD density accompanied higher defect density. Secondly, higher growth temperature has shown to be beneficial for lowering the defect density and achieving larger QD size. This was mainly due to the reduced coalescence of QDs at higher temperature. However, higher temperature led to an increase in the high In adatom diffusion length, which in turn decreased the QD density. Furthermore, having higher Sb coverage is favourable in terms of the QD morphology and density. However, it came with the cost of decreasing the sizes of QDs. Therefore, the growth conditions were determined in a way to maximise the density and the size of the QDs without significantly deteriorating the QD morphology.

Following the optimisation for the high in-plane density InAs QD growth, a high-stack (100 QD layers) InAs/GaAs QD structure with high in-plane QD density have been grown. No strain-balancing technique was applied during the growth. AFM results show high in-plane QD density even after the growth of 100 stacks of QD layers. However, TEM images show a significant decrease in the material quality as the number of QD layers increases. This is mainly due to the accumulation of the strain from the QDs, although the possibility of the growth conditions being not fully optimised due to the XRD characterisation tool not being available at the time of the growth (machine maintenance) cannot be ruled out.

Based on the calibrations carried out for the growth of high-stack InAs/GaAs QDSCs with high in-plane QD density, the epilayer structures for wafer-based regular SCs and QDSCs were grown at UCL, followed by the SC device fabrication by RBU.

EQE and *J-V* measurements under 1-sun (AM1.5) indicates that SJ SCs, with low doping level of the emitter with respect to the base, have a very low collection efficiency under a short-circuit condition. On the other hand, DJ SCs have relatively high power conversion efficiencies exceeding 16.5%. This suggests that achieving efficiency larger than 22% efficiency with DJ SC design is highly probable when ARC are applied and the grid coverage is optimised. Therefore, the good device performance achieved with DJ SCs led to the conclusion that SJ SC structure will not be considered further.

The DJ QDSCs with 20 and 50 layers of QDs exhibit inferior solar cell performances compared with the regular SCs. 50-layer QDSC display higher sub-bandgap EQE due to increased QD absorption, however, the overall device performance could not to benefit from the gain in the sub-bandgap absorption due to the loss in the supra-bandgap absorption caused by strain-induced defects. 100-layer DJ QDSC suffered from totally deteriorated EQE in both the sub-bandgap and supra-bandgap regions. This is attributed to a very high strain-induced defect density in the epilayers, which suggests the need for strain-balancing for such high-stack QDSCs.

The low SC performance of 100-layer DJ QDSC due to high density of strain-induced defects led to the conclusion that the second fabrication run of QDSCs will be focused on designs with 20 layers of QDs.

5. REFERENCES

[1] A. Luque and A. Martí, 'Increasing the Efficiency of Ideal Solar Cells by Photon Induced Transitions at Intermediate Levels', *Phys. Rev. Lett.*, vol. 78, no. 26, pp. 5014–5017, Jun. 1997.

[2] A. Marti, L. Cuadra, and A. Luque, 'Quantum dot intermediate band solar cell', in *Conference Record of the Twenty-Eighth IEEE Photovoltaic Specialists Conference, 2000*, 2000, pp. 940–943.

[3] A. Martí, E. Antolín, C. R. Stanley, C. D. Farmer, N. López, P. Díaz, E. Cánovas, P. G. Linares, and A. Luque, 'Production of Photocurrent due to Intermediate-to-Conduction-Band Transitions: A Demonstration of a Key Operating Principle of the Intermediate-Band Solar Cell', *Phys. Rev. Lett.*, vol. 97, no. 24, p. 247701, Dec. 2006.

[4] A. Luque, A. Martí, N. López, E. Antolín, E. Cánovas, C. Stanley, C. Farmer, L. J. Caballero, L. Cuadra, and J. L. Balenzategui, 'Experimental analysis of the quasi-Fermi level split in quantum dot intermediate-band solar cells', *Appl. Phys. Lett.*, vol. 87, no. 8, p. 83505, Aug. 2005.

[5] Y. Okada, T. Morioka, K. Yoshida, R. Oshima, Y. Shoji, T. Inoue, and T. Kita, 'Increase in photocurrent by optical transitions via intermediate quantum states in direct-doped InAs/GaNAs strain-compensated quantum dot solar cell', *J. Appl. Phys.*, vol. 109, no. 2, p. 24301, Jan. 2011.

[6] H. F. Lu, S. Mokkapati, L. Fu, G. Jolley, H. H. Tan, and C. Jagadish, 'Plasmonic quantum dot solar cells for enhanced infrared response', *Appl. Phys. Lett.*, vol. 100, no. 10, p. 103505, Mar. 2012.

[7] J. Wu, S. C. Mangham, V. R. Reddy, M. O. Manasreh, and B. D. Weaver, 'Surface plasmon enhanced intermediate band based quantum dots solar cell', *Sol. Energy Mater. Sol. Cells*, vol. 102, pp. 44–49, Jul. 2012.

[8] J. Wu, Z. M. Wang, V. G. Dorogan, S. Li, Z. Zhou, H. Li, J. Lee, E. S. Kim, Y. I. Mazur, and G. J. Salamo, 'Strain-free ring-shaped nanostructures by droplet epitaxy for photovoltaic application', *Appl. Phys. Lett.*, vol. 101, no. 4, p. 43904, Jul. 2012.

[9] T. Sugaya, O. Numakami, R. Oshima, S. Furue, H. Komaki, T. Amano, K. Matsubara, Y. Okano, and S. Niki, 'Ultra-high stacks of InGaAs/GaAs quantum dots for high efficiency solar cells', *Energy Environ. Sci.*, vol. 5, no. 3, pp. 6233–6237, Mar. 2012.

[10] F. K. Tutu, J. Wu, P. Lam, M. Tang, N. Miyashita, Y. Okada, J. Wilson, R. Allison, and H. Liu, 'Antimony mediated growth of high-density InAs quantum dots for photovoltaic cells', *Appl. Phys. Lett.*, vol. 103, no. 4, p. 43901, Jul. 2013.

[11] N. Kakuda, S. Tsukamoto, A. Ishii, K. Fujiwara, T. Ebisuzaki, K. Yamaguchi, and Y. Arakawa, 'Surface reconstructions on Sb-irradiated GaAs(0 0 1) formed by molecular beam epitaxy', *Microelectron. J.*, vol. 38, no. 4–5, pp. 620–624, Apr. 2007.

[12] H. Y. Liu, B. Xu, Y. H. Chen, D. Ding, and Z. G. Wang, 'Effects of seed layer on the realization of larger self-assembled coherent InAs/GaAs quantum dots', *J. Appl. Phys.*, vol. 88, no. 9, pp. 5433–5436, Nov. 2000.

[13] K.-Y. Ban, W.-K. Hong, S. P. Bremner, S. N. Dahal, H. McFelea, and C. B. Honsberg, 'Controllability of the subband occupation of InAs quantum dots on a delta-doped GaAsSb barrier', *J. Appl. Phys.*, vol. 109, no. 1, p. 14312, Jan. 2011.

[14] W.-S. Liu, H.-M. Wu, Y.-A. Liao, J.-I. Chyi, W.-Y. Chen, and T.-M. Hsu, 'High optical property vertically aligned InAs quantum dot structures with GaAsSb overgrown layers', *J. Cryst. Growth*, vol. 323, no. 1, pp. 164–166, May 2011.

[15] S. P. Bremner, K.-Y. Ban, N. N. Faleev, C. B. Honsberg, and D. J. Smith, 'Impact of stress relaxation in GaAsSb cladding layers on quantum dot creation in InAs/GaAsSb structures grown on GaAs (001)', *J. Appl. Phys.*, vol. 114, no. 10, p. 103511, Sep. 2013.